Fatigue of Materials II Advances and Emergences in Understanding
Edited by: T.S. Srivatsan, M. Ashraf Imam, and R. Srinivasan
TMS (The Minerals, Metals, & Materials Society), 2013

Influence of Austenite Stability on Steel Low Cycle Fatigue Response

G.R. Lehnhoff[1] and K.O. Findley[1]

[1]Colorado School of Mines, Metallurgical and Materials Engineering, Golden, CO USA

Keywords: TRIP Steel, Austenite Stability, Silicon and Aluminum Alloying, Low Cycle Fatigue

Abstract

Austenitic steels were subjected to tensile and total strain controlled, fully reversed axial low cycle fatigue (LCF) testing to determine the influence of stacking fault energy on austenite stability, or resistance to strain induced martensitic transformation during tensile and fatigue deformation. Expected differences in stacking fault energy were achieved by modifying alloys with different amounts of silicon and aluminum. Al alloying was found to promote martensite formation during both tensile and LCF loading, while Si was found to stabilize austenite. Martensite formation increases tensile work hardening rates, though Si additions also increase the work hardening rate without martensite transformation. Similarly, secondary cyclic strain hardening during LCF is attributed to strain induced martensite formation, but Si alloying resulted in less secondary cyclic strain hardening. The amount of secondary cyclic hardening scales linearly with martensite fraction and depends only on the martensite fraction achieved and not on the martensite (i.e. parent austenite) chemistry. Martensite formation was detrimental to LCF lives at all strain amplitudes tested, although the total amount of martensitic transformation during LCF did not always monotonically increase with strain amplitude nor correlate to the amount of tensile transformation.

Introduction

To achieve increasing fuel efficiency goals, automobile manufacturers must look to materials with better combinations of strength, ductility, and formability that allow implementation of thinner structural components and reduce vehicle weight. Materials containing metastable austenite, such as multiphase transformation induced plasticity (TRIP) steels, achieve this combination through strain induced transformation of the retained austenite to martensite. In monotonic tensile loading, the effectiveness of TRIP depends strongly on austenite stability, or resistance to strain induced transformation, as the austenite must be available to transform at higher strains where it acts to defer necking [1].

One possible way to change austenite stability is through modification of austenite stacking fault energy (SFE) because strain induced martensite nucleates on shear band intersections introduced through deformation; increasing SFE decreases the likelihood of forming distinct shear bands as cross slip becomes more prevalent [2]. As an example, the SFE effect might be manifested by exchanging silicon alloying for aluminum alloying in commercial TRIP steels to improve coatability and bainitic transformation kinetics [3,4]; Al is expected to increase SFE while Si is expected to lower or have little impact on SFE [5,6]. The literature has shown that this alloying approach does indeed influence austenite stability, although other possible underlying mechanisms include the influence of Al and Si on: phase transformation thermodynamics, carbon partitioning from bainitic ferrite into austenite during heat treatment, mechanical stress-strain partitioning between austenite and other microconstituents during loading, etc [7-11].

While the same basic mechanisms are expected to affect austenite stability and mechanical performance in both tension and fatigue, the treatment of fatigue loading is inherently more complex. For example, in stress-controlled fatigue testing, strain induced transformation is beneficial as it strengthens the microstructure and minimizes cyclic plasticity ahead of fatigue cracks [10]. However, in strain-controlled low cycle fatigue (LCF) testing, martensite formation is detrimental to fatigue life as it leads to increased stress amplitudes that promote cracking [11].

The current study aims to alter austenite SFE and stability during tensile and fatigue loading through Al and Si additions. Strain-controlled fatigue loading is of interest because components subjected to cyclic plasticity will be negatively influenced by cumulative martensitic transformation and design optimization will differ from components subjected to monotonic and/or cyclic elastic loading. Additionally, transformation during strain-controlled LCF occurs relatively uniformly in the gage section of the sample, thus facilitating martensite fraction quantification using non-destructive techniques [11-15].

Experimental Details

There are several interrelated parameters, besides austenite SFE, that can influence retained austenite stability in multiphase TRIP steels, including carbon redistribution variations near different microconstituents and stress and strain partitioning between microconstituents. To study the influence of austenite SFE on austenite stability and LCF response, fully austenitic materials with various Al and Si additions were pursued to eliminate the influences associated with non-austenitic phases. Following the microstructure survey carried out by Glenn [16], the experimental steels in Table I were cast, homogenized for 20 hours at 1200 °C, hot rolled from 76.2 mm to 15.9 mm, and solution annealed for one hour according to Table I. The Base, 2.5 Si, and 2.5 Al solution annealing temperatures were selected to achieve a constant grain size of 140 μm according to the ASTM E112 intercept method [17], thus eliminating the influence of austenite grain size on stability [18]. Figure 1 shows a light optical micrograph of the solution annealed 2.5 Si alloy and an X-ray diffraction (XRD) scan from the 2.5 Al alloy, indicating the fully austenitic structure of these materials. The 2.8 Si-L alloy (L for low nickel) is a fully austenitic alloy left over from a previous alloying scheme. Its grain size is different than the other alloys and because its Ni, C, and N content is substantially different than the other three alloys, it cannot be easily used to elucidate Al/Si alloying effects. The alloy is included in this study to provide further data for comparing mechanical behavior to austenite stability.

Table I. Experimental Steel Chemistries and Solution Annealing Temperatures

wt pct	C	N	Ni	Cr	Mn	Si	Al	S	P	Anneal T (°C)
Base	0.028	0.0034	15.05	11.06	1.09	0.002	0.05	0.001	0.002	1040
2.5 Si	0.028	0.0036	14.99	10.98	1.10	2.50	0.06	0.001	0.002	1075
2.5 Al	0.030	0.0034	15.04	11.02	1.08	0.034	2.47	0.001	0.002	1060
2.8 Si-L	0.016	0.016	13.46	10.74	0.97	2.84	0.07	0.001	0.002	1100

Following solution annealing, round bar tensile and LCF specimens were machined according to ASTM E606 with a gage length of 19.05 mm and a gage diameter of 6.35 mm [19]. Tensile tests were run at a constant displacement rate of 5 mm/min with strain being measured from an axial extensometer. LCF samples were further hand polished on a lathe to a 1 μm diamond finish and coated with epoxy to shield the specimen surface from the extensometer knife edges and prevent fatigue crack nucleation at these sites. Axial LCF tests were performed on a servo-hydraulic frame in fully-reversed (R = -1) extensometer control with a sinusoidal waveform at total strain amplitudes ranging from 0.3% to 1.2% and frequencies ranging from 0.5 Hz to 2.0 Hz, scaled inversely with amplitude. Tensile tests were interrupted at predetermined levels to assess martensite fraction evolution as a function of applied strain; LCF tests have not been interrupted to date, and martensite fractions have only been determined after cycling to failure.

Martensite fractions were determined through the use of a Fischer Feritscope® magnetic contact probe; the probe works based on the ferromagnetic nature of martensite and paramagnetic nature of austenite. Six to eight measurements were taken on each sample and averaged. Talonen *et al.* [20] have suggested that the measured martensite fractions should be multiplied by a constant value of 1.7 to account for the fact that the probes are calibrated for delta ferrite and not strain induced martensite; this correction has not been applied to the current test data because the current work does not aim to develop quantitative hardening models that require the true martensite fraction as an input.

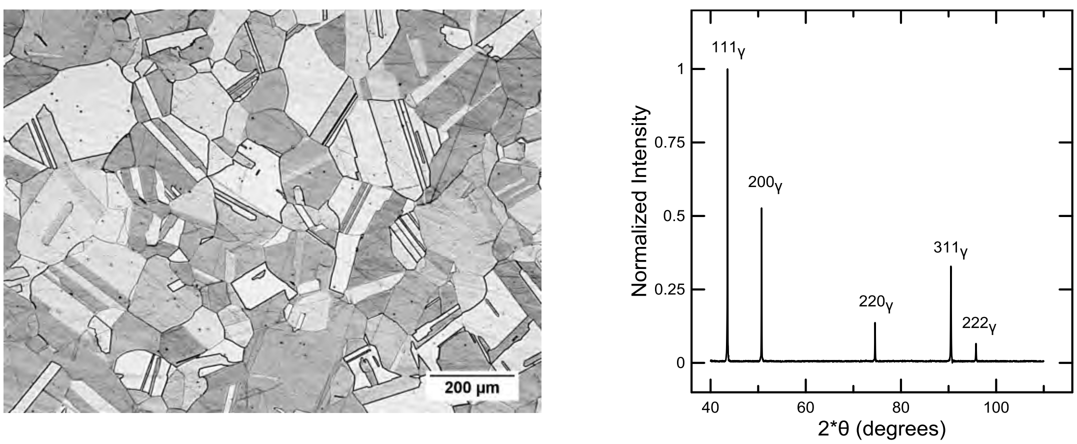

(a) (b)

Figure 1. (a) Light optical micrograph of 2.5 Si alloy showing a polycrystalline austenitic microstructure – mechanically polished to 0.05 µm alumina and etched with 80 mL ethanol, 40 mL H_2O, 40 mL HCL, and 2g $CuCl_2$. (b) XRD scan (Cu-Kα) of 2.5 Al alloy showing only austenite peaks – chemically polished for 20 minutes in a 10:10:1 mixture of H_2O, H_2O_2, and HF.

Results and Discussion

Figure 2 shows the interrupted tensile true stress-strain curves and corresponding feritscope magnetic fraction evolution curves for the four alloys. The 2.8 Si-L alloy shows the highest amount of work hardening and largest extent of martensite formation (feritscope magnetic fraction). The 2.5 Si alloy displays the next highest work hardening capacity but the lowest amount of martensite formation, suggesting that this material work hardens through an alternate mechanism besides austenite to martensite transformation. The austenite in the 2.5 Al alloy is less stable than the Base alloy and correspondingly, the 2.5 Al alloy work hardens more than the Base alloy. The same observation holds for the 2.5 Si alloy and the 2.8Si-L alloy: the 2.8 Si-L demonstrates more transformation and greater work hardening rates. The tensile martensite transformation results suggest that Al tends to destabilize austenite while Si tends to stabilize it compared to the Base alloy. However, it has been previously asserted that Al stabilizes austenite through its capacity to increase austenite SFE and thus impedes strain induced nucleation of martensite [7,21]. Transmission electron microscopy measurements of SFE for the Base, 2.5 Si, and 2.5 Al alloys are anticipated to provide additional clarity on the role of Al in the experimental alloys.

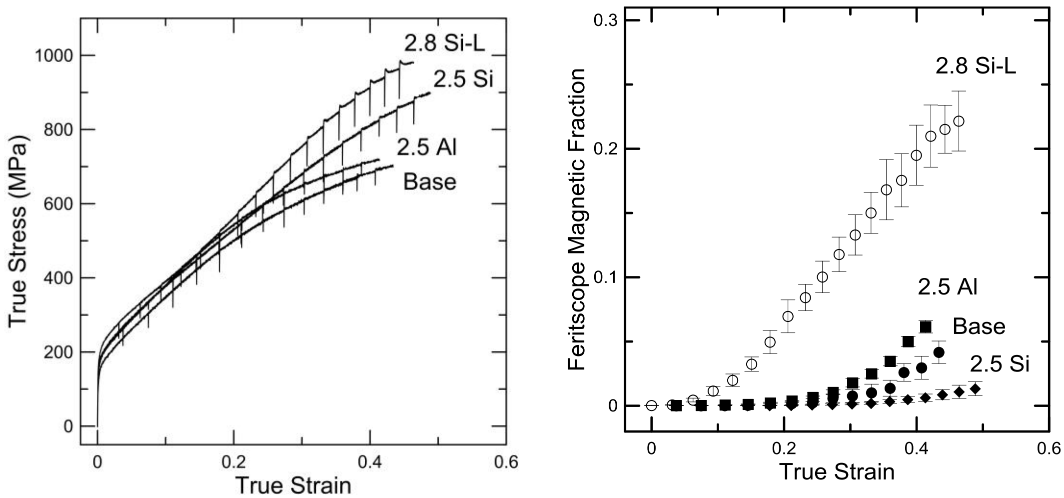

(a) (b)

Figure 2. (a) Interrupted tensile true stress-strain curves. (b) Corresponding feritscope magnetic fraction evolution as a function of true tensile strain.

Figures 3a-c show the evolution of true stress amplitude as a function of fatigue cycle number for total strain amplitudes of 0.9%, 0.6%, and 0.3%, respectively; data for the Base alloy have been excluded for clarity. Using the strain amplitude of 0.6% as an example (Figure 3b), there is an initial period of cyclic strain hardening that lasts for approximately 50 cycles followed by a plateau in stress amplitude in all three alloys. This behavior is consistent with the generation and subsequent stabilization of dislocation substructure [22]. In the case of the 2.5 Si alloy, the period of constant stress amplitude lasts until failure. However, both the 2.8 Si-L and 2.5 Al alloys show a second period of cyclic hardening that curtails the stabilization period. Secondary cyclic hardening behavior is associated with the formation of strain induced martensite. Martensite formation during fatigue loading is known to require a certain cyclic incubation period during which sufficient martensite nucleation sites are generated in the microstructure [14]. The same general cyclic deformation behavior is also observed at strain amplitudes of 0.9% and 0.3%, as shown respectively in Figures 3a and 3c, although the amounts and rates of hardening are amplitude dependent.

Figure 3d shows the relationship between maximum stress amplitude achieved during LCF life and the feritscope magnetic fraction determined after failure. There is a direct correlation between maximum stress amplitude and martensite fraction at all strain amplitudes, again indicating martensite formation is the cause of secondary cyclic hardening. Furthermore, the correlation between cyclic hardening and martensite fraction appears roughly linear, thus implying that it may be possible to capture cyclic hardening due to martensite formation using a simple linear rule of mixtures mechanical model [23]. Also, the maximum stress amplitudes as a function of martensite fraction of all of the alloys appear to collapse to a single line for a given strain amplitude, which implies that martensite fraction alone, and not martensite chemistry (which is the same as the parent austenite chemistry), controls the hardening behavior in this alloy system. However, Hahnenberger *et al.* have shown that martensite composition may play a bigger role in other alloy systems where the austenite carbon content has been altered through the addition of carbide-forming elements such as Ti and Nb [13].

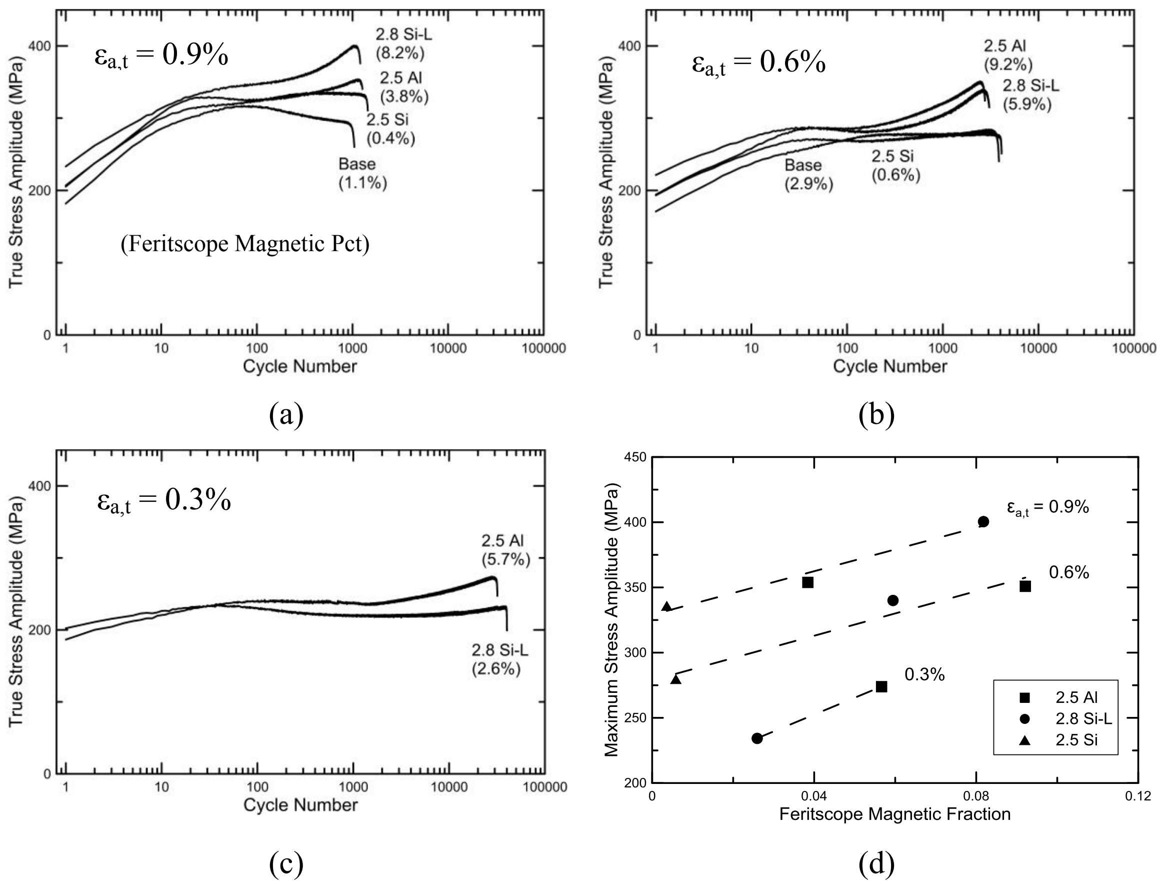

Figure 3. Evolution of true stress amplitude vs. cycle number for the various alloys tested at total strain amplitudes of (a) $\varepsilon_{a,t}$ = 0.9%, (b) 0.6%, and (c) 0.3%. Magnetic percents at failure measured by feritscope are in parentheses. (d) Correlation between maximum stress amplitude and magnetic fraction at failure for each strain amplitude.

The strain hardening behavior during tensile and fatigue loading is not consistent across all of the alloy conditions. Specifically, the 2.5 Si alloy shows appreciable tensile work hardening, due to a mechanism other than martensitic formation, but essentially no secondary cyclic hardening because it does not undergo significant transformation in fatigue. The difference between tensile and fatigue behavior suggests that the work hardening mechanisms operative in tension are not triggered during fatigue loading in this material. Furthermore, the propensity for a material to transform in tension does not necessarily correspond to its tendency to transform in fatigue. For example, the 2.8 Si-L alloy transforms much more readily in tension than the 2.5 Al alloy (Figure 2b), but during LCF at total strain amplitudes of 0.3% and 0.6%, the 2.5 Al alloy transforms more than the 2.8 Si-L alloy (Figure 4a). The 2.5 Al alloy accordingly experiences more secondary cyclic hardening than the 2.8 Si-L alloy at these levels (Figures 3b-d) despite its lower tensile work hardening capacity (Figure 2a). Understanding how tensile work hardening mechanisms translate to fatigue loading conditions may be a crucial consideration for successful implementation of advanced steels in applications subject to monotonic and fatigue design requirements.

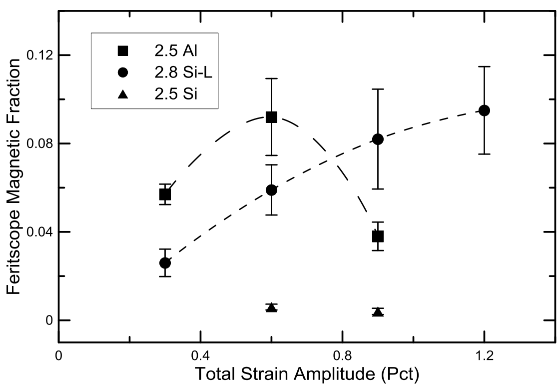

(a)

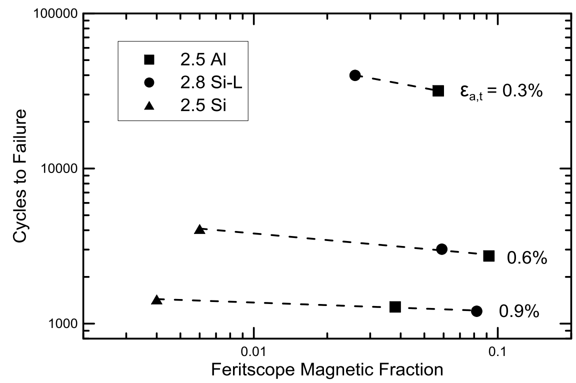

(b)

Figure 4. (a) Dependence of magnetic fraction on total strain amplitude. (b) Dependence of LCF life on magnetic fraction measured at failure for three different total strain amplitudes showing that martensite formation is detrimental to LCF life.

Figure 4a shows the dependence of martensite transformation on applied strain amplitude. The 2.5 Al alloy shows a distinct maximum in martensite fraction near a strain amplitude of 0.6%, and the 2.8 Si-L alloy appears to approach a maximum amount of transformation at the highest amplitude tested. The Base (not shown in Figure 4a) and 2.5 Si alloys seem to behave in a similar qualitative manner to the 2.5 Al alloy, but additional data points are required. The concave nature of martensite fraction as a function of strain amplitude indicates that at lower strain amplitudes the generated dislocation substructure is ineffective at nucleating martensite while at higher strain amplitudes, fatigue failure occurs more rapidly and shortens the secondary hardening regime.

Figure 4b shows the dependence of LCF life on magnetic fraction measured at failure for three different total strain amplitudes. At all strain amplitudes, martensite formation is detrimental to LCF life. Martensite formation increases the stress amplitude during strain-controlled fatigue cycling, thus increasing the driving force for damage initiation and propagation during the tensile portion of the cycle [24].

Conclusions

Metastable austenitic stainless steels were tested in tension and low cycle fatigue and characterized with respect to the amount of strain-induced martensitic transformation. The following results and conclusions were obtained:

1. Aluminum present in austenite promotes strain induced martensitic transformation during tensile and LCF loading while silicon inhibits transformation.
2. Martensite formation increases tensile work hardening, but in the case of the 2.5 Si alloy, high work hardening was achieved with minimal martensite formation.

3. Maximum stress amplitude reached during the LCF life scales linearly with martensite fraction measured at failure such that secondary cyclic hardening is attributable to martensite formation.
4. Secondary cyclic hardening depends only on the amount of martensite formed and not the martensite (i.e. parent austenite) chemistry for the alloys tested.
5. Tensile transformation and work hardening capacity do not necessarily correspond to martensite formation during LCF and secondary cyclic hardening.
6. The amount of martensite formed at failure does not continuously increase with strain amplitude if failure inhibits the total amount of transformation possible.
7. Martensite formation is detrimental to LCF life at all of the strain amplitudes tested.

Acknowledgments

This material is based upon work supported by the National Science Foundation under Grant No. 0955236. This research was supported in part by an award from the Department of Energy (DOE) Office of Science Graduate Fellowship Program (DOE SCGF). The DOE SCGF Program was made possible in part by the American Recovery and Reinvestment Act of 2009. The DOE SCGF program is administered by the Oak Ridge Institute for Science and Education for the DOE. ORISE is managed by Oak Ridge Associated Universities (ORAU) under DOE contract number DE-AC05-06OR23100. All opinions expressed in this paper are the authors' and do not necessarily reflect the policies and views of DOE, ORAU, or ORISE. The authors also gratefully acknowledge the support of AK Steel and the Advanced Steel Processing and Products Research Center, a university-industry cooperative research center.

References

1. G.B. Olson, "Transformation Plasticity and the Stability of Plastic Flow," *Deformation, Processing, and Structure*, ed. G. Krauss (Metals Park, OH: ASM, 1984) 391-425.

2. G.B. Olson and M. Cohen, "Kinetics of Strain-Induced Martensitic Nucleation," *Metallurgical Transactions A,* 6 (1975), 791-795.

3. J. Mahieu, S. Claessens, and B.C. De Cooman, "Galvanizability of High-Strength Steels for Automotive Applications," *Met. Mat. Trans A*, 32 (2001), 2905-2908.

4. J. Mahieu, J. Maki, B.C. De Cooman, and S. Claessens, "Phase Transformation and Mechanical Properties of Si-Free CMnAl Transformation-Induced Plasticity–Aided Steel," *Metallurgical and Materials Transactions A*, 33 (2002), 2573-2580.

5. A. Dumay, J.-P. Chateau, S. Allain, S. Migot, O. Bouaziz, "Influence of Addition Elements on the Stacking-Fault Energy and Mechanical Properties of an Austenitic Fe–Mn–C Steel," *Materials Science and Engineering A,* 483–484 (2008), 184–187.

6. R.E. Schramm and R.P. Reed, "Stacking Fault Energies of Seven Commercial Austenitic Stainless Steels," *Metallurgical Transactions A*, 6 (1975), 1345-1351.

7. L. Samek, E. De Moor, J. Penning, and B.C. De Cooman, "Influence of Alloying Elements on the Kinetics of Strain-Induced Martensitic Nucleation in Low-Alloy, Multiphase High-Strength Steels," *Metallurgical and Materials Transactions A*, 37 (2006), 109-124.

8. A.K. De, R.S. Kircher, J.G. Speer, and D.K. Matlock, "Transformation Behavior of Retained Austenite in TRIP Steels as Revealed by a Specialized Etching Technique," *Proceedings of the International Conference on Advanced High Strength Sheet Steels for Automotive Applications*, ed. J.G. Speer (Warrendale, PA: AIST, 2004) 337-347.

9. P.J. Jacques, J. Ladriere, and F. Delannay, "On the Influence of Interactions between Phases on the Mechanical Stability of Retained Austenite in Transformation-Induced Plasticity Multiphase Steels," *Metallurgical and Materials Transactions A*, 32 (2001), 2759-2768.

10. G.B. Olson, R. Chait, M. Azrin, and R.A. Gagne, "Fatigue Strength of TRIP Steels," *Metallurgical Transactions A*, 11 (1980), 1069-1071.

11. M. Smaga, F. Walther, and D. Eifler, "Investigation and Modelling of the Plasticity-Induced Martensite Formation in Metastable Austenites," *Int. J. Mat. Res.*, 97 (2006), 1648-1655.

12. M. Smaga, F. Walther, and D. Eifler, "Deformation-Induced Martensitic Transformation in Metastable Austenitic Steels," *Materials Science and Engineering A*, 483-484 (2008), 394-397.

13. F. Hahnenberger, M. Smaga, and D. Eifler, "Influence of γ-α'-Phase Transformation in Metastable Austenitic Steels on the Mechanical Behavior during Tensile and Fatigue Loading at Ambient and Lower Temperatures," *Adv. Eng. Materials*, doi: 10.1002/adem.201100341 (2012).

14. A. Glage, A. Weidner, and H. Biermann, "Effect of Austenite Stability on the Low Cycle Fatigue Behavior and Microstructure of High Alloyed Metastable Austenitic Cast TRIP Steels," *Procedia Engineering*, 2 (2010), 2085-2094.

15. A. Das, S. Sivaprasad, P.C. Chakraborti, and S. Tarafder, "Morphologies and Characteristics of Deformation Induced Martensite during Low Cycle Fatigue Behaviour of Austenitic Stainless Steel," *Materials Science and Engineering A*, 528 (2011), 7909-7914.

16. M.L. Glenn, "The Prediction of Microstructure in Low-Chromium Substitutes for Stainless Steels," *Journal of Materials Engineering*, 10 (1988), 181-191.

17. Standard Test Methods for Determining Average Grain Size, ASTM Standard E112 (2004).

18. A.K. De, D.C. Murdock, M.C. Mataya, J.G. Speer, and D.K. Matlock, "Quantitative Measurement of Deformation-Induced Martensite in 304 Stainless Steel by X-Ray Diffraction," *Scripta Materialia*, 50 (2004), 1445-1449.

19. Standard Practice for Strain-Controlled Fatigue Testing, ASTM Standard E606 (2004).

20. J. Talonen, P. Aspegren, and H. Hanninen, "Comparison of Different Methods for Measuring Strain Induced Martensite Content in Austenitic Steels," *Mat. Sci. Tech.*, 20 (2004), 1506-1512.

21. E. Jimenez-Melero, N.H. van Dijk, L. Zhao, J. Sietsma, S.E. Offerman, J.P. Wright, and S. van der Zwaag, "The Effect of Aluminum and Phosphorus on the Stability of Individual Austenite Grains in TRIP Steels," *Acta Materialia*, 57 (2009), 533-543.

22. H-J Christ, "Cyclic Stress-Strain Response and Microstructure," *ASM Handbook Vol. 19: Fatigue and Fracture*, ed. S.R. Lampman (Metals Park, OH: ASM International, 1996) 73-95.

23. G.R. Lehnhoff and K.O. Findley, "Influence of Austenite Stability on Predicted Cyclic Stress-Strain Response of Metastable Austenitic Steels," *Procedia Eng.*, 10 (2011), 1097-1102.

24. G. Baudry and A. Pineau, "Influence of Strain-induced Martensitic Transformation on the Low-Cycle Fatigue Behavior of a Stainless Steel," *Mat. Sci. Eng.*, 28 (1977), 229-242.